J. Fluid Mech. (1982), *vol.* 122, *pp.* 251–271
Printed in Great Britain

Numerical study of viscous flow in rotating rectangular ducts

By CHARLES G. SPEZIALE
Stevens Institute of Technology, Hoboken, NJ 07030

(Received 21 September 1981 and in revised form 23 February 1982)

A numerical study of the laminar flow of an incompressible viscous fluid in rotating ducts of rectangular cross-section is conducted. The full time-dependent nonlinear equations of motion are solved by finite-difference techniques for moderate to relatively rapid rotation rates where both the convective and viscous terms play an important role. At weak to moderate rotation rates, a double-vortex secondary flow appears in the transverse planes of the duct whose structure is relatively independent of the aspect ratio of the duct. For Rossby numbers $Ro < 100$ this secondary flow is shown to lead to substantial distortions of the axial velocity profiles. For more rapid rotations ($Ro < 1$), the secondary flow (in a duct with an aspect ratio of two) is shown to split into an asymmetric configuration of four counter-rotating vortices similar to that which appears in curved ducts. It is demonstrated mathematically that this effect could result from a disparity in the symmetry of the convective and Coriolis terms in the equations of motion. If the rotation rates are increased further, the secondary flow restabilizes to a slightly asymmetric double-vortex configuration and the axial velocity assumes a Taylor–Proudman configuration in the interior of the duct. Comparisons with existing experimental results are quite favourable.

1. Introduction

The development of secondary flows in pressure-driven flow through a straight pipe or duct that is subjected to a rigid rotation has long been recognized. Here the axis of rotation is perpendicular to the axial direction of the pipe or duct, which is long enough so that end effects can be suppressed. Consequently, the secondary flow is independent of the co-ordinate along the axial direction. The earliest work on this subject consisted of theoretical investigations of the weak-rotation case for laminar flow in circular pipes. Barua (1954), by using a perturbation approach, showed that for weak rotations the secondary flow consisted of a counter-rotating double-vortex configuration similar to that which occurs in a stationary curved pipe. He also derived a formula for the associated rise in the resistance coefficient of the pipe. A short time later, Benton (1956) calculated the effect of the Earth's rotation on laminar flow in circular pipes. By using a perturbation expansion, he showed that the secondary flow consisted of the same type of double-vortex configuration that Barua had found. In addition, Benton calculated the distortion of the usual parabolic velocity profile that results from the presence of secondary flow. However, he was not able to observe the secondary flow directly since it was very weak. Subsequent to this study, Benton & Boyer (1966) examined the case of laminar flow in a rapidly rotating duct of arbitrary cross-section.

This problem is not as difficult as the moderate rotation case since the flow in the interior of duct is approximately geostrophic.

During the past decade, most of the research on this subject has been focused on the study of roll-cell instabilities or turbulence in rotating rectangular channels. For laminar flow in a rotating rectangular channel, Hart (1971) proved experimentally and theoretically (using a linear stability analysis) that at relatively rapid rotation rates an instability exists in the form of longitudinal roll cells of non-dimensional wavenumber five. At higher rotation rates, the flow restabilizes to a Taylor–Proudman regime where the gradient of the axial velocity along the axis of rotation in the interior of the channel is zero. Hart also showed that the problem of the stability of rotating channel flow is analogous to the stability of a temperature-stratified fluid. Johnston, Halleen & Lezius (1972) and Lezius & Johnston (1976) made a more comprehensive study of Taylor-type roll-cell instabilities for laminar and turbulent flows in a rotating channel. By using a linear stability analysis, they found that the critical disturbance mode for laminar flow occurred at a Reynolds number of 88·53 and a rotation number (i.e. the inverse Rossby number) of 0·5. At higher Reynolds numbers, they found instabilities for a range of rotation numbers between 0 and 3. Lezius & Johnston (1976) found that the onset of roll-cell instabilities for turbulent flow with Reynolds numbers between 6000 and 35000 occurred at a rotation rate of 0·022 – a value which was in excellent agreement with the experiments that they conducted.

Wagner & Velkoff (1972) conducted measurements for turbulent flow in a rotating rectangular duct and examined the developing flow from the entrance of the duct. More recently, there have been some numerical studies of turbulent flow in rotating rectangular ducts. Majumdar, Pratap & Spalding (1977) used the k-ϵ model of turbulence and were able to obtain some results that were in good agreement with experiments for weak rotations. Howard, Patankar & Bordynuik (1980) conducted further calculations with a modified k-ϵ model where the effects of rotation were accounted for empirically in the transport equations for the turbulent kinetic energy and scalar dissipation rate. However, although these calculations do represent an important first step, more research is needed on turbulence modelling before this problem can be calculated in an accurate fashion.

In this paper, we will conduct a detailed numerical study of laminar flow in rotating rectangular ducts at moderate to relatively rapid rotation rates where both the convective and diffusive terms play an important role and, consequently, the full nonlinear equations of motion must be solved. As mentioned earlier, all of the previous calculations on rotating duct flow dealt with the two simplified limiting cases (i.e. with weak rotations or with strong rotations) or with the stability of channel flow (i.e. a large-aspect-ratio duct). We will concentrate our attention on the structure of the secondary flow and its effect on the axial flow in a low-aspect-ratio duct for a variety of Reynolds numbers and rotation rates. In order to test the numerical method used, the weak-rotation problem will be briefly studied first. For this case, it is shown that the usual counter-rotating double-vortex configuration for the secondary flow (where the lengthscale of the vortices is of the order of the width of the duct) occurs *independently* of the aspect ratio of the duct. However, as the rotation rate is substantially increased, this double-vortex configuration breaks down into an asymmetric configuration of four counter-rotating vortices that could result from a disparity in the symmetry of the convective and Coriolis terms. This occurs at relatively rapid rotation

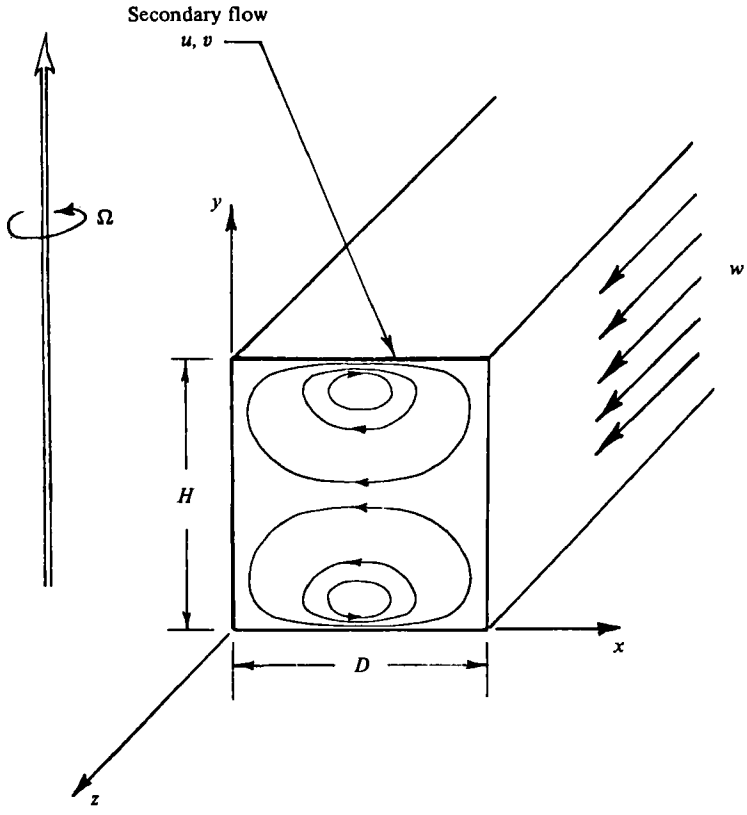

FIGURE 1. Secondary flow in a rotating rectangular channel as given in Hart (1971).

rates (i.e. Rossby numbers of the order one). Further increases in the rotation rate lead to a restabilization of the secondary flow into a slightly asymmetric double-vortex configuration where the axial velocity assumes a Taylor–Proudman configuration in the interior of the channel. No previous calculations on rotating duct flow covered the Taylor–Proudman regime in detail. Also, in contrast to previous studies, we will calculate the time-dependent evolution of the secondary flow. Comparisons with existing experimental data and the prospects for future research will be discussed later.

2. Formulation of the physical problem

The problem to be considered is that of the laminar flow of an incompressible viscous fluid in a straight rectangular duct that is subjected to a steady rotation Ω. Here, the axis of rotation is perpendicular to the span of the duct (see figure 1) and the axial pressure gradient $\partial P/\partial z = -G$ is constant and is maintained by external means (P is the modified pressure, which includes the gravitational and centrifugal force potentials). The duct is sufficiently long so that there exists a central section of the duct where end effects are suppressed and the flow properties are independent of the axial co-ordinate z. In the absence of rotations, the fully developed velocity field $\mathbf{v}$ is of the unidirectional form

$$\mathbf{v} = \{0, 0, v_z(x, y)\}, \tag{2.1}$$

where v_z is determined from the Poisson equation (cf. Batchelor 1967)

$$\nabla^2 v_z = -G/\mu. \tag{2.2}$$

Equation (2.2), in which μ denotes the shear viscosity of the fluid, is solved subject to the no-slip condition that v_z vanishes on the walls of the duct. This yields the classical quasi-parabolic profile for the axial velocity v_z. However, for non-zero rotation rates, the fully-developed velocity field is *three-dimensional* relative to an observer who rotates with the duct (cf. Hart 1971), i.e. $\mathbf{v}$ is of the form

$$\mathbf{v} = \{v_x(x,y), v_y(x,y), v_z(x,y)\}, \tag{2.3}$$

where v_x and v_y constitute the secondary flow. The vector velocity $\mathbf{v}$ is a solution of the Navier–Stokes equation and the continuity equation, which (relative to an observer who is rotating with the duct) take the form

$$\frac{\partial \mathbf{v}}{\partial t} + \mathbf{v}.\nabla\mathbf{v} = -\frac{1}{\rho}\nabla P + \nu\nabla^2\mathbf{v} - 2\boldsymbol{\Omega}\times\mathbf{v}, \quad \nabla.\mathbf{v} = 0, \tag{2.4}$$

where ρ is the density of the fluid, $\nu \equiv \mu/\rho$ is the kinematic viscosity, $\boldsymbol{\Omega} = \Omega\mathbf{j}$ is the rotation rate of the duct, and P is the modified pressure, which satisfies the constraint

$$\partial P/\partial z = -G. \tag{2.5}$$

Here, the time-dependent form of the Navier–Stokes equation has been maintained since we are going to study the evolution of the flow in time. By making use of (2.5) and the fact that the flow properties are independent of the axial co-ordinate z, (2.4) takes the form

$$\frac{\partial u}{\partial t} + u\frac{\partial u}{\partial x} + v\frac{\partial u}{\partial y} = -\frac{1}{\rho}\frac{\partial P}{\partial x} + \nu\nabla^2 u - 2\Omega w, \tag{2.6a}$$

$$\frac{\partial v}{\partial t} + u\frac{\partial v}{\partial x} + v\frac{\partial v}{\partial y} = -\frac{1}{\rho}\frac{\partial P}{\partial y} + \nu\nabla^2 v, \tag{2.6b}$$

$$\frac{\partial w}{\partial t} + u\frac{\partial w}{\partial x} + v\frac{\partial w}{\partial y} = \frac{G}{\rho} + \nu\nabla^2 w + 2\Omega u, \tag{2.6c}$$

$$\frac{\partial u}{\partial x} + \frac{\partial v}{\partial y} = 0, \tag{2.6d}$$

where

$$u \equiv v_x, \quad v \equiv v_y, \quad w \equiv v_z. \tag{2.7}$$

As a result of the simplified form of the continuity equation (2.6d), there exists a stream function ψ for the secondary flow such that

$$u = -\frac{\partial \psi}{\partial y}, \quad v = \frac{\partial \psi}{\partial x}. \tag{2.8}$$

Here ψ is a solution of the Poisson equation

$$\nabla^2\psi = \omega, \tag{2.9}$$

since

$$\omega \equiv \omega_z = \frac{\partial v}{\partial x} - \frac{\partial u}{\partial y} \tag{2.10}$$

is the axial component of the vorticity. The axial vorticity ω is determined from the z-component of the vorticity transport equation, which is given by

$$\frac{\partial \omega}{\partial t}+u\frac{\partial \omega}{\partial x}+v\frac{\partial \omega}{\partial y}=\nu\nabla^2\omega+2\Omega\frac{\partial w}{\partial y}. \tag{2.11}$$

Equation (2.11) is obtained by taking the difference between the derivative of (2.6*b*) with respect to x and the derivative of (2.6*a*) with respect to y. As a result of (2.9) it is quite clear that secondary flows result from a non-zero axial vorticity ω. Consequently, it is obvious that the Coriolis term $2\Omega\,\partial w/\partial y$, which serves as an axial vorticity source term in (2.11), is the driving mechanism for the creation of secondary flow in a rotating duct.

Since the flow properties depend on only two spatial co-ordinates, a modified vorticity–streamfunction approach was chosen for this numerical study. More specifically, the axial momentum equation (2.6*c*) will be solved numerically coupled with the axial vorticity transport equation (2.11), the Poisson equation (2.9) for the secondary flow, and the secondary-flow velocity relations (2.8). The problem will be cast in dimensionless form by the use of a lengthscale D and a velocity scale W_0, which are, respectively, the width of the duct (see figure 1) and the integrated average axial velocity. In dimensionless form, the governing equations to be solved take the form

$$\frac{\partial w}{\partial t}+u\frac{\partial w}{\partial x}+v\frac{\partial w}{\partial y}=C+\frac{1}{Re}\nabla^2 w+\frac{1}{Ro}u, \tag{2.12a}$$

$$\frac{\partial \omega}{\partial t}+u\frac{\partial \omega}{\partial x}+v\frac{\partial \omega}{\partial y}=\frac{1}{Re}\nabla^2\omega+\frac{1}{Ro}\frac{\partial w}{\partial y}, \tag{2.12b}$$

$$\nabla^2\psi=\omega, \tag{2.12c}$$

$$u=-\frac{\partial \psi}{\partial y},\quad v=\frac{\partial \psi}{\partial x}, \tag{2.12d, e}$$

where all of the field variables are scaled with respect to W_0 and D. In (2.12), C is the dimensionless pressure gradient, Re is the Reynolds number, and Ro is the Rossby number, which are given respectively by

$$C=\frac{GD}{\rho W_0^2},\quad Re=\frac{W_0 D}{\nu},\quad Ro=\frac{W_0}{2\Omega D}. \tag{2.13}$$

At this point, we will introduce another dimensionless number, namely the Ekman number E, which is given by

$$E=\frac{\nu}{2\Omega D^2},$$

and will be of use for the comparisons with experimental data that will be made later.

The coupled system of nonlinear partial differential equations (2.12) is solved subject to the boundary conditions

$$u=0,\quad v=0,\quad w=0,\quad \psi=0, \tag{2.14}$$

on the walls of the duct. The boundary conditions on the axial vorticity ω must be derived (i.e. they will be obtained by a Taylor expansion), and we will do that in §3. In so far as the initial conditions are concerned, two different problems will be

considered. We will consider the problem of starting flow where the pressure gradient $-G$ is impulsively applied in a steadily rotating framework. For starting flow, the initial conditions for (2.12) are

$$u = 0, \quad v = 0, \quad w = 0, \quad \omega = 0, \quad \psi = 0 \tag{2.15}$$

at $t = 0$. The other initial-value problem to be considered is that of fully-developed laminar flow in a stationary duct that is subjected to an impulsively applied angular velocity. For this problem, the initial conditions that must be applied to (2.12) are

$$u = 0, \quad v = 0, \quad w = w_1, \quad \omega = 0, \quad \psi = 0, \tag{2.16}$$

at $t = 0$, where w_1 is the classical quasi-parabolic velocity profile obtained from (2.2). Of course, both initial-value problems have the *same* steady-state solution. In §3 a detailed discussion of the numerical approach used will be presented.

3. Numerical approach

Since the geometry of the problem is rectangular, the finite-difference method was used where the cross-section of the duct was discretized into an $M \times N$ rectangular grid. The axial momentum and vorticity transport equations (2.12a, b) were solved by a modified form of Arakawa's method that utilizes the DuFort–Frankel scheme for the diffusion terms. Arakawa's method is advantageous since it is a fourth-order-accurate explicit-difference scheme which has no boundary-condition problems (see Roache 1972). The scheme, within the context of this problem, conserves ω, ω^2, w, and w^2 (as well as the total kinetic energy) and is, furthermore, not subject to nonlinear instabilities that arise from aliasing errors (all aliasing errors are bounded). In Arakawa's method, the convective derivative of any field variable Φ is represented as follows:

$$\begin{aligned}
\left(\frac{D\Phi}{Dt}\right)^n_{i,j} &\equiv \left(\frac{\partial\Phi}{\partial t} + u\frac{\partial\Phi}{\partial x} + v\frac{\partial\Phi}{\partial y}\right)^n_{i,j} \\
&= \frac{\Phi^{n+1}_{i,j} - \Phi^{n-1}_{i,j}}{2\Delta t} - \frac{1}{12\,\Delta x\,\Delta y}[\psi^n_{i+1,j} - \psi^n_{i-1,j})\,(\Phi^n_{i,j+1} - \Phi^n_{i,j-1}) \\
&\quad - (\psi^n_{i,j+1} - \psi^n_{i,j-1})\,(\Phi^n_{i+1,j} - \Phi^n_{i-1,j}) \\
&\quad + \psi^n_{i+1,j}(\Phi^n_{i+1,j+1} - \Phi^n_{i+1,j-1}) - \psi^n_{i-1,j}(\Phi^n_{i-1,j+1} - \Phi^n_{i-1,j-1}) \\
&\quad - \psi^n_{i,j+1}(\Phi^n_{i+1,j+1} - \Phi^n_{i-1,j+1}) \\
&\quad + \psi^n_{i,j-1}(\Phi^n_{i+1,j-1} - \Phi^n_{i-1,j-1}) + \Phi^n_{i,j+1}(\psi^n_{i+1,j+1} - \psi^n_{i-1,j+1}) \\
&\quad - \Phi^n_{i,j-1}(\psi^n_{i+1,j-1} - \psi^n_{i-1,j-1}) \\
&\quad - \Phi^n_{i+1,j}(\psi^n_{i+1,j+1} - \psi^n_{i+1,j-1}) + \Phi^n_{i-1,j}(\psi^n_{i-1,j+1} - \psi^n_{i-1,j-1})],
\end{aligned} \tag{3.1}$$

where Δx and Δy are respectively the grid lengths in the x- and y-directions, Δt is the time interval, and

$$\Phi^n_{i,j} \equiv \Phi(i\Delta x, j\Delta y, n\Delta t), \quad \psi^n_{i,j} \equiv \psi(i\Delta x, j\Delta y, n\Delta t)$$
$$(n = 0, 1, \ldots, \quad i = 0, 1, \ldots, M, \quad j = 0, 1, \ldots, N). \tag{3.2}$$

The axial momentum equation and vorticity-transport equation are solved in the finite-difference form

$$\left(\frac{Dw}{Dt}\right)^n_{i,j} = C + \frac{1}{Re}\left[\frac{w^n_{i+1,j} - w^{n-1}_{i,j} - w^{n+1}_{i,j} + w^n_{i-1,j}}{(\Delta x)^2} + \frac{w^n_{i,j+1} - w^{n-1}_{i,j} - w^{n+1}_{i,j} + w^n_{i,j-1}}{(\Delta y)^2}\right] + \frac{1}{Ro}u^n_{i,j}, \quad (3.3a)$$

$$\left(\frac{D\omega}{Dt}\right)^n_{i,j} = \frac{1}{Re}\left[\frac{\omega^n_{i+1,j} - \omega^{n-1}_{i,j} - \omega^{n+1}_{i,j} + \omega^n_{i-1,j}}{(\Delta x)^2} + \frac{\omega^n_{i,j+1} - \omega^{n-1}_{i,j} - \omega^{n+1}_{i,j} + \omega^n_{i,j-1}}{(\Delta y)^2}\right] + \frac{1}{Ro}\left(\frac{w^n_{i,j+1} - w^n_{i,j-1}}{2\Delta y}\right), \quad (3.3b)$$

where the convective derivatives are formulated by Arakawa's method (3.1). The viscous-diffusion terms are formulated with the DuFort–Frankel scheme, which is second-order accurate (see Roache 1972). For stability purposes, the Coriolis terms are centred in time and the spatial derivative of w is central-differenced for second-order accuracy. It should be clear to the reader that (3.3) constitutes an explicit finite-difference scheme.

The Poisson equation (2.12*c*) is solved in the standard second-order-accurate finite-difference form

$$\frac{\psi^n_{i+1,j} - 2\psi^n_{i,j} + \psi^n_{i-1,j}}{(\Delta x)^2} + \frac{\psi^n_{i,j+1} - 2\psi^n_{i,j} + \psi^n_{i,j-1}}{(\Delta y)^2} = \omega^n_{i,j}. \quad (3.4)$$

The solution of (3.4) is accomplished by using a compact non-iterative Poisson solver due to Buneman (1969) that employs cyclic reduction. This Poisson solver is extremely efficient since it was constructed for use in rectangular domains and suffers only from the minor inconvenience of requiring that M and N be powers of 2. The secondary-flow velocities, which are determined from (2.12*d*), are solved in the second-order-accurate central-difference form

$$u^n_{i,j} = -\left(\frac{\psi^n_{i,j+1} - \psi^n_{i,j-1}}{2\Delta y}\right), \quad v^n_{i,j} = \left(\frac{\psi^n_{i+1,j} - \psi^n_{i-1,j}}{2\Delta x}\right). \quad (3.5)$$

Equations (3.3)–(3.5) represent the complete finite-difference formulation of the governing equations of motion (2.12). These equations are supplemented with the boundary conditions (2.14) and the initial conditions (2.15) or (2.16). As mentioned earlier, the boundary conditions for the axial vorticity must be derived. This was accomplished by a second-order-accurate Taylor expansion of (2.12*c*) in the vicinity of the walls of the duct, which yields the boundary conditions

$$\omega^n_{0,j} = \frac{8\psi^n_{1,j} - \psi^n_{2,j}}{2(\Delta x)^2}, \quad \omega^n_{M,j} = \frac{8\psi^n_{M-1,j} - \psi^n_{M-2,j}}{2(\Delta x)^2}, \quad (3.6a, b)$$

$$\omega^n_{i,0} = \frac{8\psi^n_{i,1} - \psi^n_{i,2}}{2(\Delta y)^2}, \quad \omega^n_{i,N} = \frac{8\psi^n_{i,N-1} - \psi^n_{i,N-2}}{2(\Delta y)^2}. \quad (3.6c, d)$$

After each iteration, the boundary conditions on ω must be updated by using (3.6). It should be quite clear that the complete formulation of the problem is second-order accurate, i.e. the truncation error τ goes as

$$\|\tau\| = O(\Delta t^2, \Delta x^2, \Delta y^2) \quad (3.7)$$

where $\|\ \|$ denotes any suitable norm.

Calculations were conducted for 2×1 ducts and 8×1 ducts (i.e. ducts with an aspect ratio H/D of 2 and 8), the latter of which is quite often used to simulate channel flow experimentally (cf. Hart 1971). A 2×1 duct was chosen since it has the smallest aspect ratio that allows for the development of vortices whose characteristic length (in any direction) is of the order of the width of the duct – a property that the secondary flow has in ducts with larger aspect ratios. For the 2×1 duct, we selected either $M = 16$ and $N = 32$ or $M = 32$ and $N = 64$, depending on the strength of the rotation (M and N must be powers of two in order to use the high-speed Poisson solver). For the 8×1 duct, we selected $M = 16$ and $N = 128$. The stability criterion used was the standard one obtained by a simple superposition of the generalized CFL condition and von Neumann stability criterion, which are derived from a local linearized stability analysis. More specifically, Δt was chosen to satisfy the constraint

$$\Delta t \leqslant \left[\frac{2}{Re}\left(\frac{1}{\Delta x^2}+\frac{1}{\Delta y^2}\right)+\frac{|u|_{\max}}{\Delta x}+\frac{|v|_{\max}}{\Delta y}\right]^{-1}, \tag{3.8}$$

which in practice was applied with a safety factor of two. For most of the calculations conducted, convergence to three significant figures was obtained in 600 to 2000 iterations, the latter number representing the extreme case when the secondary flow was strong so that (3.8) became more restrictive. These calculations required from 5 min to 1 h on a DEC system-10 computer.

Calculations were conducted for a variety of Reynolds numbers and Rossby numbers, mostly in the ranges

$$0 < Re < 500, \quad 10^{-1} < Ro < 10^{2}. \tag{3.9}$$

Consequently, the flow was strongly laminar and the rotation rates were moderate to relatively rapid (namely, in the intermediate range between negligibly weak rotations and strong rotational geostrophic flow). For water (at room temperature) flowing in a duct with a width $D = 1{\cdot}92$ in with the physical properties $\nu = 1{\cdot}1 \times 10^{-5}\,\mathrm{ft^2/s}$, and $\rho = 1{\cdot}936\,\mathrm{slugs/ft^3}$ these Rossby numbers correspond to the following range of rotation rates:

$$10^{-4} < \Omega < 1\,(\mathrm{rad/s}). \tag{3.10}$$

In §4 we will examine the numerical results obtained in complete detail.

4. Numerical results and comparisons with experiments

Initially, we examined the time-dependent evolution of secondary flow in a 2×1 duct for the problem of starting flow in a rotating framework. In figures 2(*a–d*), computer-generated contour maps of the streamlines relative to an observer looking upstream are shown at various times for $Re = 86$ and $Ro = 1{\cdot}85$ corresponding to the fully-developed rotating flow. Dimensional values of time as well as those for the angular velocity correspond to water (at room temperature) flowing in a duct with a characteristic length $D \simeq 2$ in. These values of Ω will be useful later in studying the effect of a continuous increase in angular velocity on a given axial flow. It is quite clear that these calculations indicate that the secondary flow starts as a double-vortex configuration that is strongly compressed against the upper and lower walls of the duct. This compressed double-vortex secondary flow then diffuses to the interior of the duct where it assumes a fully-developed configuration (see figure 2*d*) that is in

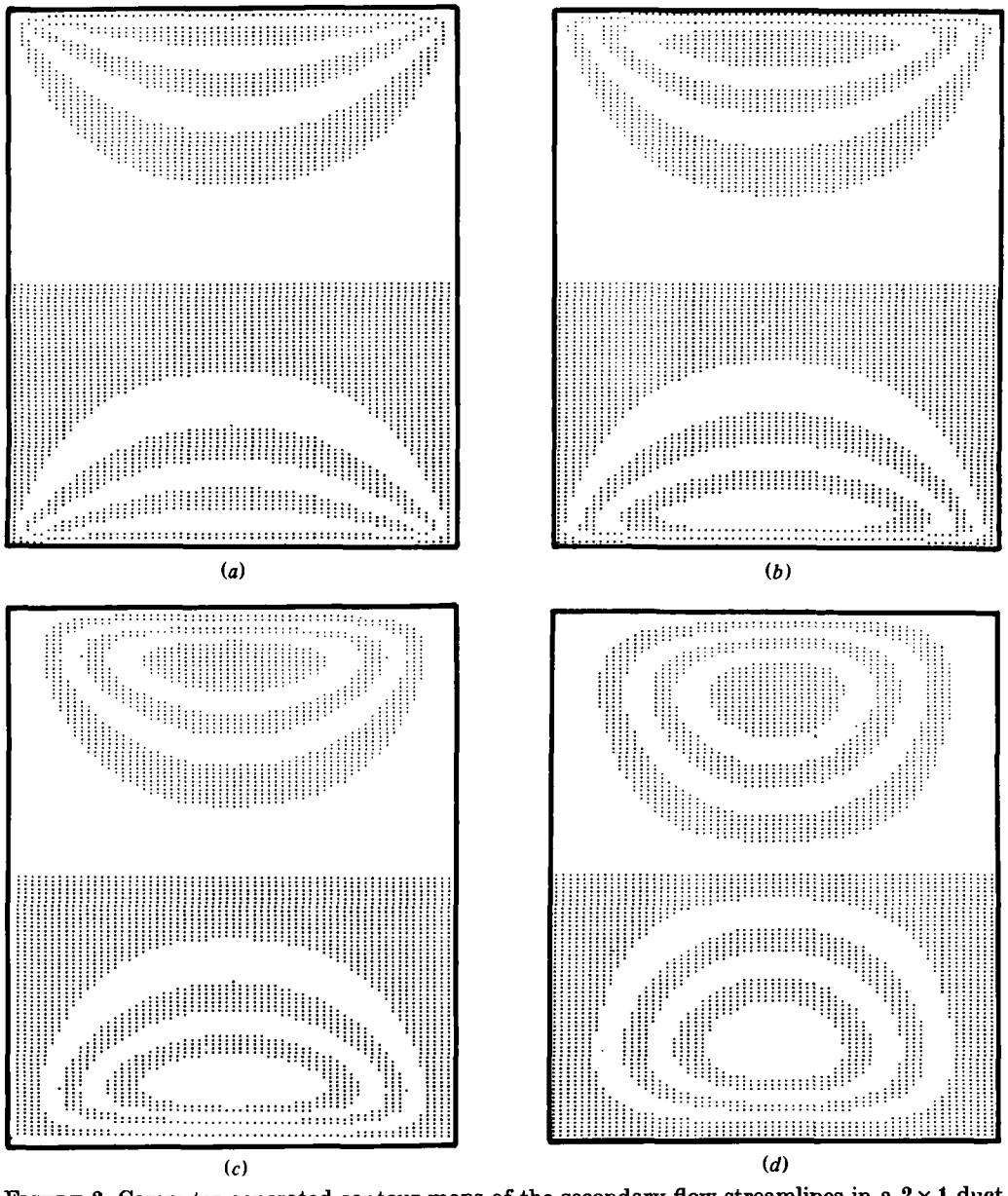

FIGURE 2. Computer-generated contour maps of the secondary-flow streamlines in a 2×1 duct at various times for starting flow. $Re = 86$, $Ro = 1{\cdot}85$ ($\Omega = 0{\cdot}01$ rad/s, $G = 1 \times 10^{-4}$ lb/ft^3). (*a*) $t = 1$ s, (*b*) 5 s, (*c*) 25 s, (*d*) fully-developed.

excellent qualitative agreement with the calculations of Hart (1971) shown in figure 1. Approximately 600 s were required to obtain a fully-developed flow (i.e. convergence to three significant figures); however, most of the qualitative changes occur in the first 100 s. The reader should note that for all of the computer-generated contour maps presented in this paper, a vortex on a shaded background indicates a counterclockwise rotation and a vortex on a white background indicates a clockwise rotation. Furthermore, since these contour maps were produced on the line printer, the aspect ratio of

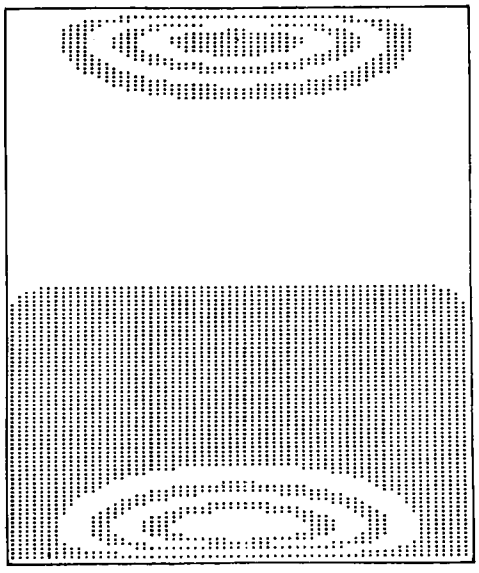

FIGURE 3. Computer-generated contour map of the fully-developed secondary flow streamlines in an 8×1 duct. $Re = 107$, $Ro = 2{\cdot}3 \times 10^3$ ($\Omega = 10^{-5}$ rad/s, $G = 6 \times 10^{-5}$ lb/ft^3).

the channel was not made to scale because of the considerable inconvenience that would be involved. However, this has little ill effect since the streamline patterns only serve the purpose of providing a mechanism to observe the qualitative structure of the secondary flow.

Calculations were conducted for an 8×1 duct (which is quite often used to simulate channel flow) for $Re = 107$ and $Ro = 2{\cdot}3 \times 10^3$, which constitutes a weak rotation. Again, the fully-developed secondary-flow streamlines (which are shown in figure 3) consist of a counter-rotating double-vortex configuration (one vortex located at the upper and lower wall) where each vortex has a uniform lengthscale of the order of the width of the duct D. These calculations, along with those conducted for intermediate cases, indicate that this is true for *any* duct with an aspect ratio $H/D \geqslant 2$ which is subjected to weak or moderate rotations. However, when more rapid rotations are applied to a large-aspect-ratio duct this double-vortex secondary flow spreads a larger distance into the interior of the duct. To illustrate this point, the fully-developed secondary flow in an 8×1 duct for $Re = 105$ and $Ro = 2{\cdot}25$ is shown in figure 4. This is a stable, but relatively rapid, rotation (according to the results of Lezius & Johnston (1976) this flow would become unstable to longitudinal roll cells when $Ro \simeq 2{\cdot}0$). It is quite clear in this case that the secondary flow has a significant effect in a horizontal layer of thickness $2D$ (twice the distance for the weak to moderate rotation case) near the upper and lower walls of the duct. Thus, the magnitude of the secondary flow relative to the axial flow near the horizontal centreline of the 8×1 duct is substantially larger here than for the weak- to moderate-rotation case. Specific numerical values are as follows:

$$(a)\quad \tfrac{1}{3}H < y < \tfrac{2}{3}H, \quad Re = 107, \quad Ro = 2{\cdot}3 \times 10^3, \quad \frac{|u, v|_{\max}}{w_{\max}} = 4 \times 10^{-7}; \quad (4.1)$$

$$(b)\quad \tfrac{1}{3}H < y < \tfrac{2}{3}H, \quad Re = 105, \quad Ro = 2{\cdot}25, \quad \frac{|u, v|_{\max}}{w_{\max}} = 3 \times 10^{-3}. \quad (4.2)$$

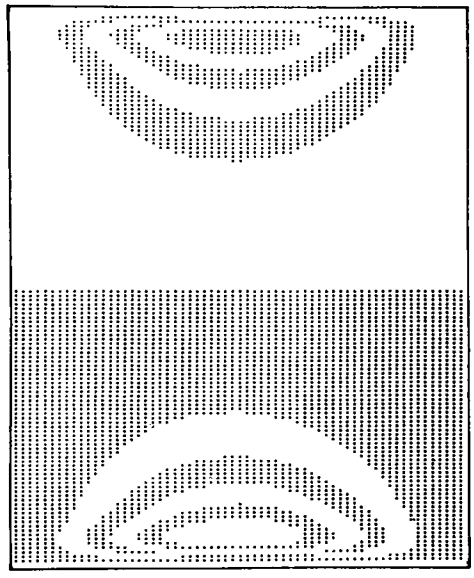

FIGURE 4. Computer-generated contour map of the fully-developed secondary-flow streamlines in an 8×1 duct. $Re = 105$, $Ro = 2{\cdot}25$ ($\Omega = 0{\cdot}01$ rad/s, $G = 6 \times 10^{-5}$ lb/ft^3).

Since the calculations conducted here indicate that the magnitude of the secondary flow must be of the order of 1 % of the axial flow to have a significant effect, they do support the usual assumption made in experiments that secondary flows are of little consequence near the centreline of a duct whose aspect ratio exceeds 6 or 7.

Now, we will examine the effect of moderate to relatively rapid rotations on the axial flow in a 2×1 duct. In figure 5, the ratio of the flowrate Q for a stationary duct to the flowrate Q_r for a rotating duct (with the same applied pressure gradient) is plotted versus the Reynolds number of the rotating flow for various rotation rates Ω. The range of Reynolds numbers $0 < Re < 100$ for these rotation rates correspond to the range of Rossby numbers $0 < Ro < 2{\cdot}15$. It is quite clear that the rotations lead to a substantial reduction in the flow rate of amounts varying from 10–50 %. Unfortunately, no theoretical or experimental results were available on the rectangular duct for comparisons. However, as shown in figure 5, for low Reynolds numbers and rotation rates the numerical values obtained for Q/Q_r are in the range of those values obtained by Barua (1954) for a circular pipe. While a direct comparison cannot be made between the precise numerical values of both cases because of the difference in geometry, one would expect the values to be in the same range as a result of the similarity in the structure of the two flows (i.e. the axial velocity in the duct is quasi-parabolic and the secondary flow consists of two counter-rotating vortices as in the case of the circular pipe).

The fully-developed axial-velocity profiles at the horizontal and vertical centrelines of the 2×1 duct are shown in figures 6(a, b) for $Re = 235$ and $Ro = 50{\cdot}5$ ($\Omega = 0{\cdot}001$ rad/s). It is quite clear that the secondary flow causes a noticeable distortion in these profiles even though its magnitude is only approximately 1 % of that of the axial flow. The axial velocity at the horizontal centreline of the duct (shown in figure 6a) is asymmetric with its maximum velocity shifted toward the low-pressure side of the duct (i.e. the side of the duct closest to the axis of rotation), consistent with

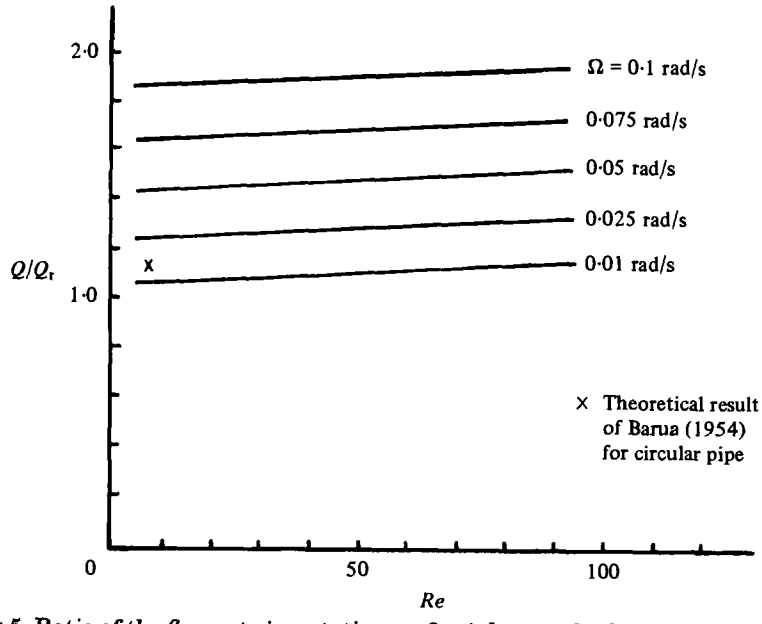

FIGURE 5. Ratio of the flow rate in a stationary 2 × 1 duct to the flow rate in a rotating 2 × 1 duct as a function of the Reynolds number and the rotation rate.

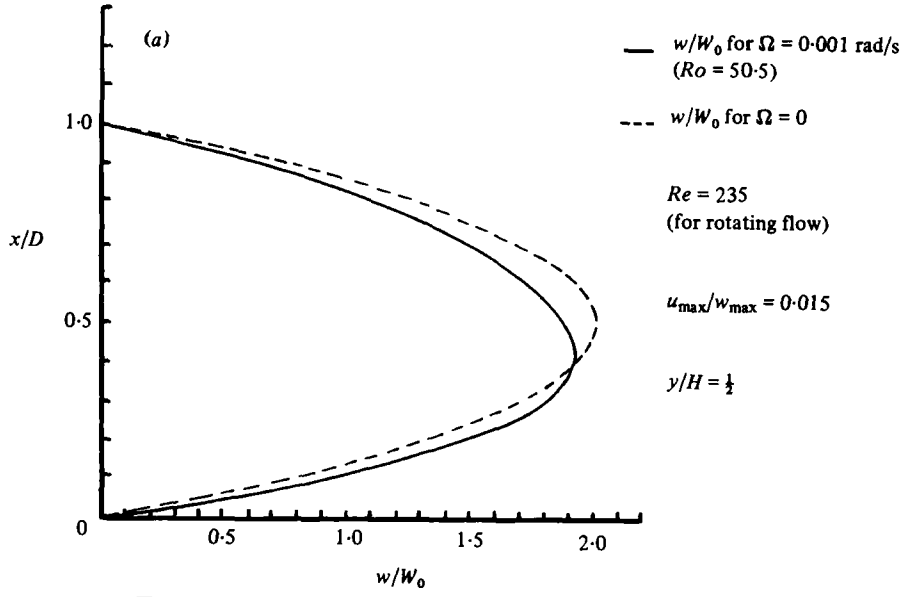

FIGURE 6 (*a*). For caption see facing page.

the results of Benton (1956) and Lezius & Johnston (1976). The axial velocity at the vertical centreline of the duct is symmetric but begins to flatten in the central region of the duct (see figure 6*b*). From the governing equations of motion (2.12) it is a simple matter to show that the axial velocity must be symmetric about the centre of any vertical axis in the duct. In figures 6 (*a*, *b*), the corresponding laminar velocity profiles are also shown in the absence of rotations. Consistent with the previous results, there

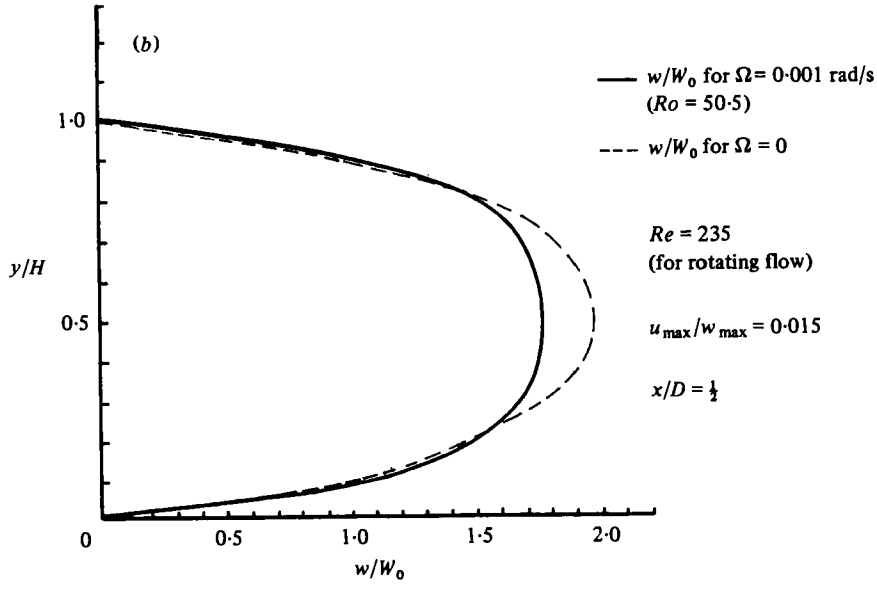

FIGURE 6. Axial-velocity profiles in a 2×1 duct for $Re = 235$ and $Ro = 50{\cdot}5$ ($\Omega = 0{\cdot}001$ rad/s, $G = 2{\cdot}5 \times 10^{-4}$ lb/ft^3): (*a*) along the horizontal centreline of the duct; (*b*) along the vertical centreline of the duct.

is a noticeable decrease in the flowrate through the duct. The same corresponding axial-velocity profiles are shown in figures 7(*a*, *b*) for a 2×1 duct with $Re = 86$ and $Ro = 1{\cdot}85$ ($\Omega = 0{\cdot}01$ rad/s). Since, for this case, the magnitude of the secondary flow is approximately 7 % of that of the axial flow the distortions just discussed are even more striking. More specifically, the axial velocity at the horizontal centreline of the duct is highly asymmetric, the axial velocity at the vertical centreline of the duct is noticeably flattened in the central portion of the duct, and there is a substantial reduction in the flow rate. For both of these cases, the secondary flow consists of the same type of double-vortex configuration shown in figure 2(*d*).

When the rotations become more rapid (i.e. $Ro < 1$) and the Reynolds number is large enough, the double-vortex configuration for the secondary flow in a 2×1 duct breaks down into a configuration of four counter-rotating vortices that is asymmetric with respect to the vertical centreline of the duct. This probably results from a disparity in the symmetry of the convective and Coriolis terms (combined with the viscous terms) corresponding to the standard double-vortex secondary flow. More specifically, for a *weak* double-vortex secondary flow, the flow field has the following symmetries (in a strong approximate sense) relative to an (x, y)-co-ordinate system with origin at the geometric centre of the duct:

$$\left.\begin{aligned} &\omega(x, y) = \omega(-x, y), \quad \omega(x, y) = -\omega(x, -y), \\ &u(x, y) = u(-x, y), \quad u(x, y) = u(x, -y), \\ &v(x, y) = -v(-x, y), \quad v(x, y) = -v(x, -y), \\ &w(x, y) = w(-x, y), \quad w(x, y) = w(x, -y). \end{aligned}\right\} \tag{4.3}$$

Furthermore, the derivative of a symmetric function with respect to a given variable is antisymmetric with respect to that variable and vice versa, e.g.

$$\frac{\partial w}{\partial y}(x, y) = -\frac{\partial w}{\partial y}(x, -y). \tag{4.4}$$

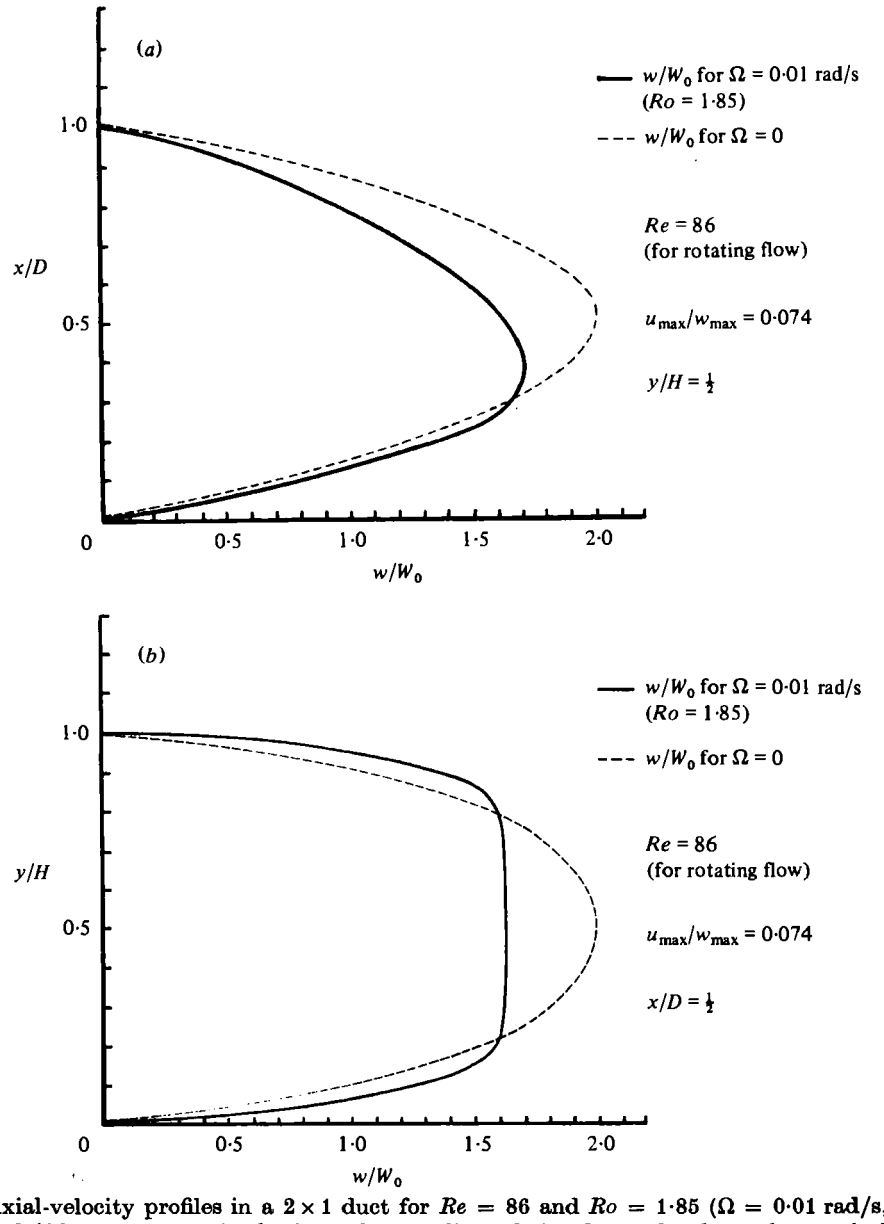

FIGURE 7. Axial-velocity profiles in a 2×1 duct for $Re = 86$ and $Ro = 1{\cdot}85$ ($\Omega = 0{\cdot}01$ rad/s, $G = 1 \times 10^{-4}$ lb/ft^3): (a) along the horizontal centreline of the duct; (b) along the vertical centreline of the duct.

Consequently, the right-hand side of (2.12b) given by

$$\text{RHS} \equiv \frac{1}{Re}\nabla^2\omega + \frac{1}{Ro}\frac{\partial w}{\partial y} \tag{4.5}$$

has the same symmetry properties as ω and $\partial\omega/\partial t$, i.e.

$$\text{RHS}(x, y) = \text{RHS}(-x, y), \quad \text{RHS}(x, y) = -\text{RHS}(x, -y). \tag{4.6}$$

However, the convective terms in (2.12*b*),

$$\frac{\delta\omega}{\delta t} = u\frac{\partial\omega}{\partial x} + v\frac{\partial\omega}{\partial y}, \tag{4.7}$$

have a different symmetry. From (4.3) it is a simple matter to show that $\delta\omega/\delta t$ is an antisymmetric function of x and y, i.e.

$$\frac{\delta\omega}{\delta t}(x, y) = -\frac{\delta\omega}{\delta t}(-x, y), \quad \frac{\delta\omega}{\delta t}(x, y) = -\frac{\delta\omega}{\delta t}(x, -y). \tag{4.8}$$

Thus, when the convective terms play an important role, the vorticity field will no longer be approximately symmetric about the vertical centreline of the duct, and the classical symmetric double-vortex configuration shown in figure 1 will cease to be a solution to the governing equations. The calculations conducted herein indicate that this occurs when

$$Ro \sim 1, \quad Re \gg 1,$$

which is within the range of Ro and Re when longitudinal roll cells occur in rotating channel flow (see Lezius & Johnston 1976). At this point, it should be noted that, as a result of the symmetry of u in (4.3*b*), it is quite clear from (2.12*a*) that the asymmetry of the axial-velocity profiles along the horizontal centreline of the duct must be a consequence of the convective terms. This asymmetry in the axial-velocity profiles surfaces at higher Rossby numbers since the convective terms in the axial momentum equation (2.12*a*) are linear in the secondary flow velocities, unlike in the axial vorticity-transport equation.

Now, we will present numerical results that illustrate the breakdown of the double-vortex secondary flow and we will examine its effect on the axial flow. In figures 8 (*a–d*), computer-generated secondary-flow streamlines are shown, at various times, for an initially fully-developed laminar flow in a stationary 2×1 duct that is subjected to an impulsive rotation ($\Omega = 0{\cdot}1$ rad/s). The resulting fully-developed rotating flow corresponds to $Re = 279$ and $Ro = 0{\cdot}6$. From these results, it is quite clear that in this case the secondary flow starts as a double-vortex configuration and then breaks down into a configuration of four counter-rotating vortices that are *not* symmetric with respect to the vertical centreline of the duct (see figure 8*d*). This resulting secondary flow is almost identical with that obtained in curved rectangular ducts at higher Dean numbers as shown in figure 9 (see Cheng, Lin & Ou 1976). There is no question that this flow is real, since the same results were obtained when the grid was refined (with the time step reduced) and when the flow field was perturbed during the calculation. Consequently, this secondary-flow configuration is stable with respect to disturbances in the transverse plane of the duct. The axial-velocity profiles at the horizontal and vertical centrelines of the duct are shown respectively in figures 10 (*a*, *b*). Again, the axial velocity at the horizontal centreline of the duct (see figure 10*a*) is substantially distorted, with its maximum velocity shifted toward the low-pressure side of the duct. However, a point of inflexion occurs on the high-pressure side of the duct (which may be indicative of an instability with respect to longitudinally varying disturbances) similar to that which occurs in a curved rectangular duct (see Cheng *et al.* 1976). This is the side of the duct where longitudinal roll cells occur in rotating channel flow. The axial-velocity profile at the vertical centreline of the duct (see figure 10*b*) is symmetric and flat with the exception of peaks located near the upper and lower walls of the duct

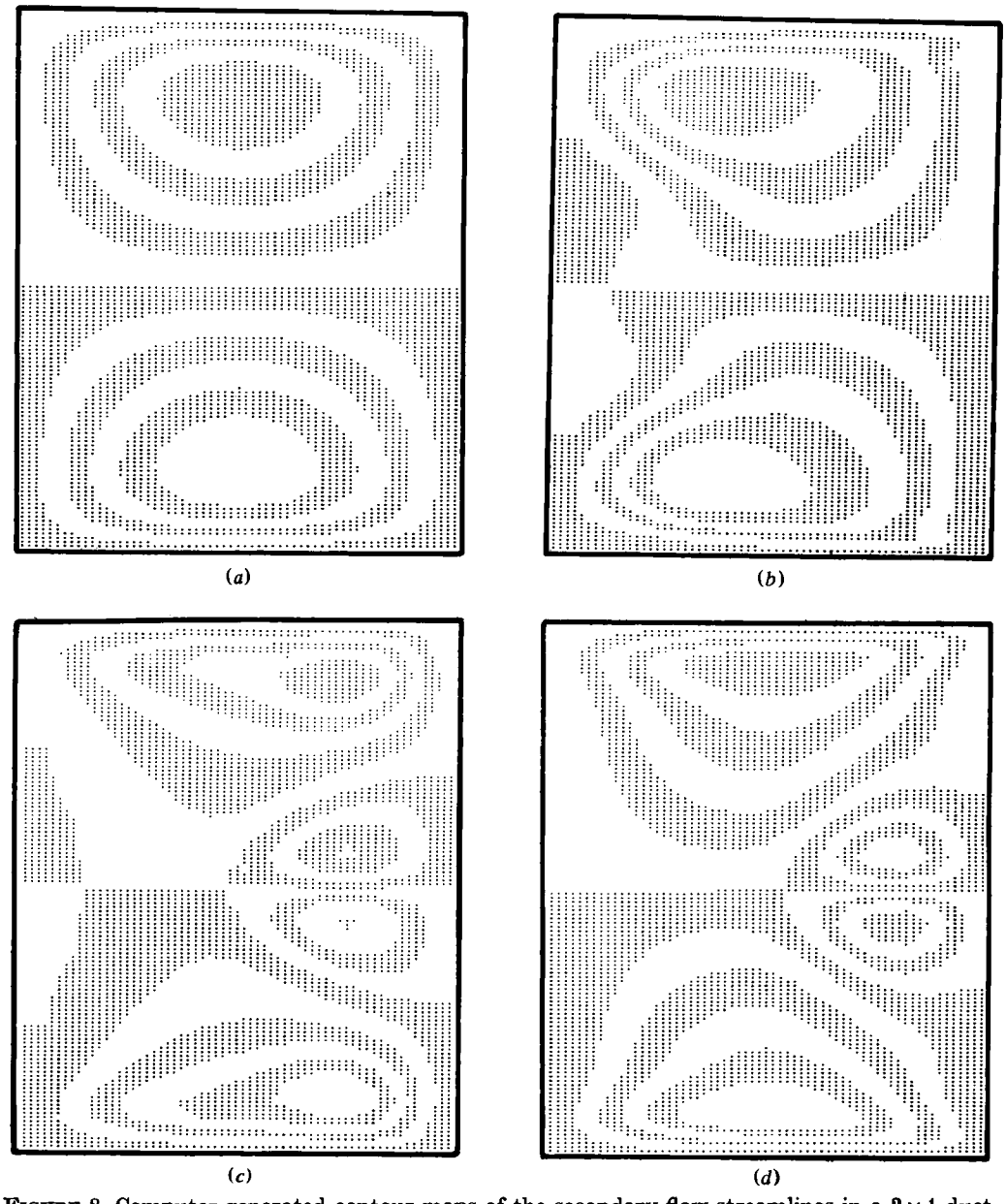

FIGURE 8. Computer-generated contour maps of the secondary-flow streamlines in a 2×1 duct at various times for an initially fully-developed flow subjected to an impulsively applied rotation. $Re = 279$, $Ro = 0{\cdot}6$ ($\Omega = 0{\cdot}1$ rad/s, $G = 6 \times 10^{-4}$ lb/ft^3): (*a*) $t = 1$ s, (*b*) 12·5 s, (*c*) 75 s, (*d*) fully-developed.

and at its centreline. This profile is similar to those obtained for rotating channel flow in the presence of longitudinal roll cells (see Hart 1971).

If the angular velocity of the duct is now increased to $\Omega = 0{\cdot}2$ rad/s while maintaining the same pressure gradient (this yields $Re = 220$ and $Ro = 0{\cdot}24$ for the fully-developed rotating flow) the subsidiary counter-rotating vortex pair that was present on the high-pressure side of the duct (see figure 8*d*) disappears and the secondary flow

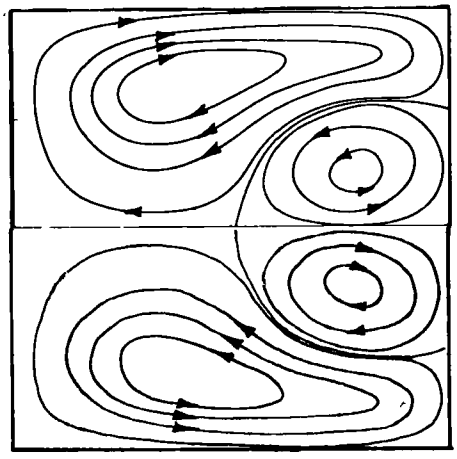

FIGURE 9. Secondary-flow streamlines in a curved square duct obtained by Cheng *et al.* (1976).

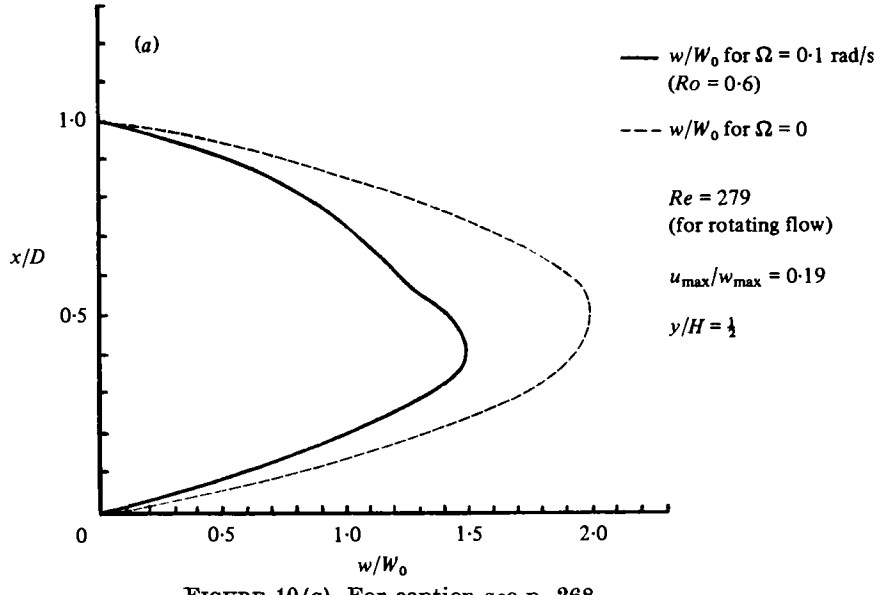

FIGURE 10(*a*). For caption see p. 268.

restabilizes to a slightly asymmetric double-vortex configuration as shown in figure 11. Furthermore, the point of inflexion in the axial-velocity profile along the horizontal centreline of the duct disappears (see figure 12*a*). The axial-velocity profile along the vertical centreline of the duct (shown in figure 12*b*) assumes a Taylor–Proudman configuration in the interior of the duct (i.e. the axial velocity does not vary along the direction of the axis of rotation in the interior of the duct). The two peaks in this axial-velocity profile near the upper and lower walls of the duct have their maximum values at a distance approximately equal to $2E^{\frac{1}{2}}D$ from each wall, which is consistent with the position of the overshoot obtained from the theory of the linear Ekman layer (see Hart 1971). This is not surprising since at relatively rapid rotations the secondary

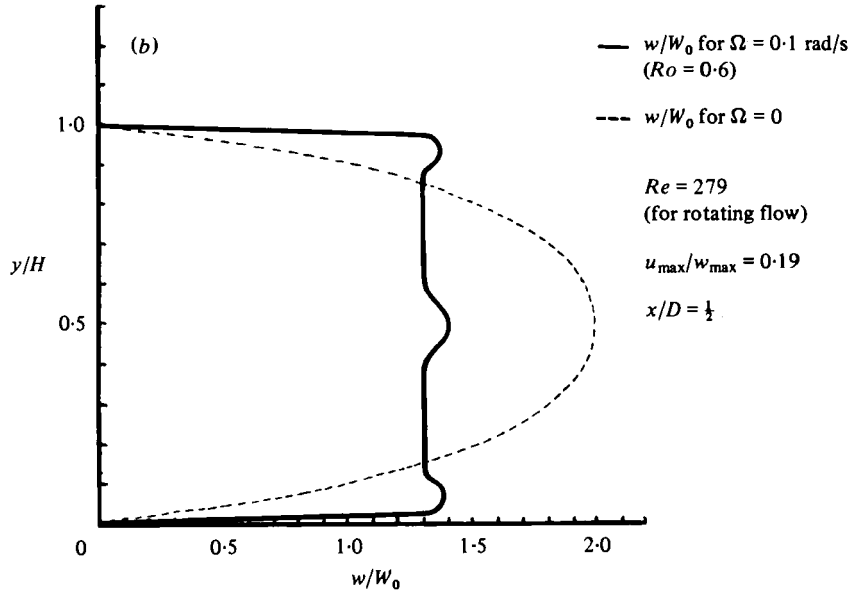

FIGURE 10. Axial-velocity profiles in a 2×1 duct for $Re = 279$ and $Ro = 0{\cdot}6$ ($\Omega = 0{\cdot}1$ rad/s, $G = 6 \times 10^{-4}$ lb/ft^3): (*a*) along the horizontal centreline of the duct; (*b*) along the vertical centreline of the duct.

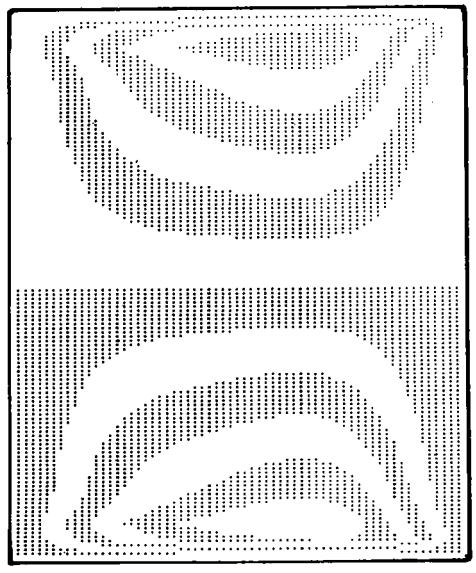

FIGURE 11. Computer-generated contour map of the fully-developed secondary flow streamlines in a 2×1 duct. $Re = 220$, $Ro = 0{\cdot}24$ ($\Omega = 0{\cdot}2$ rad/s, $G = 6 \times 10^{-4}$ lb/ft^3).

flow can be thought of as originating from Ekman suction as discussed in Hart (1971). The axial-velocity profile along the vertical centreline of the duct obtained numerically is thus in excellent qualitative agreement with experiments (see Hart 1971, figure 4*e*). To the best knowledge of the author, these are the first complete calculations to illustrate the restabilization of flow in a rotating rectangular duct to a Taylor–Proudman regime.

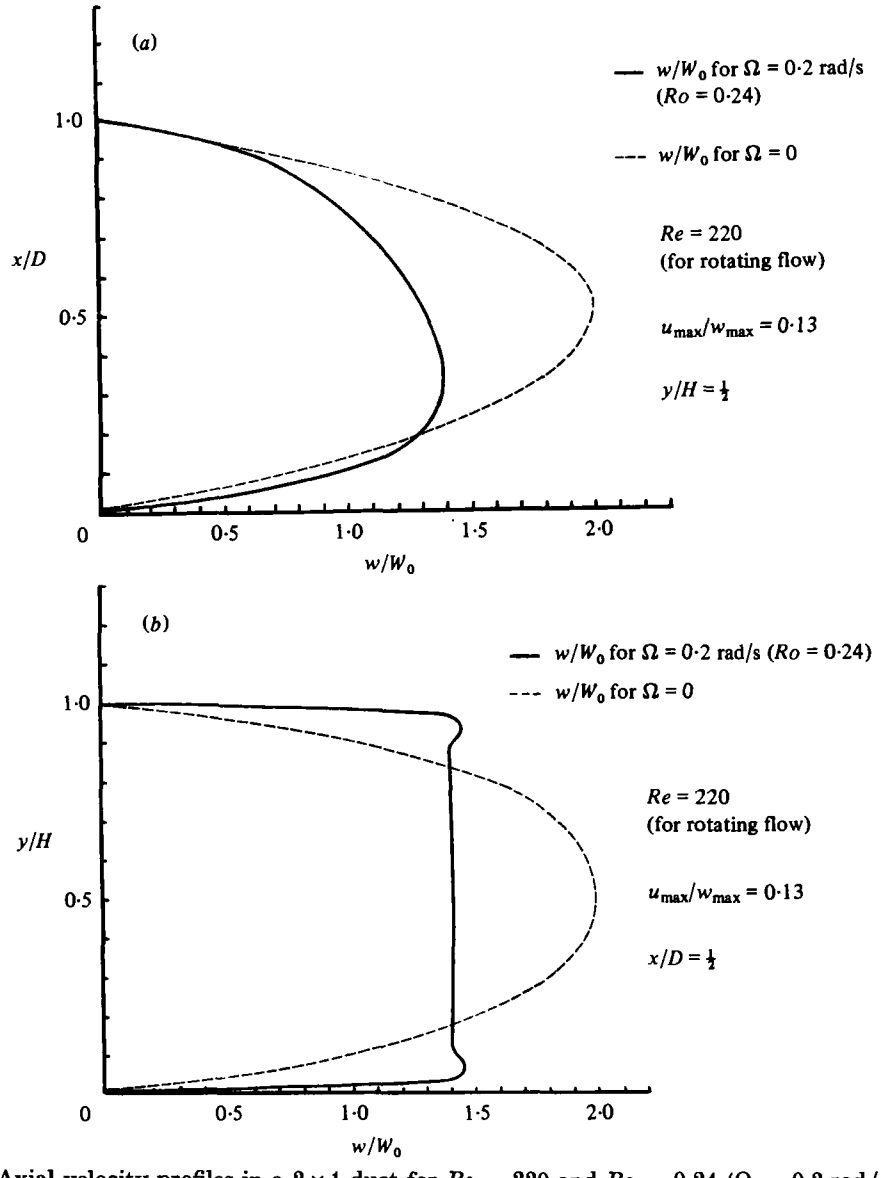

FIGURE 12. Axial-velocity profiles in a 2×1 duct for $Re = 220$ and $Ro = 0{\cdot}24$ ($\Omega = 0{\cdot}2$ rad/s, $G = 6 \times 10^{-4}$ lb/ft^3): (*a*) along the horizontal centreline of the duct; (*b*) along the vertical centreline of the duct.

5. Summary and conclusions

A numerical study of laminar flow in rotating rectangular ducts has been conducted utilizing finite-difference techniques. For weak to moderate rotation rates (with $H/D \geqslant 2$) it was shown that the resulting secondary flow consists of a counter-rotating double-vortex configuration (one vortex located at the upper and lower walls of the duct) where the diameter of the vortices is of the order of the width D of the duct. Provided that the Rossby number $Ro > 100$, the secondary flow was found to have only a mild distortional effect on the axial velocity. A thorough study of the effect of

secondary flow on the axial velocity in a 2×1 duct was conducted for $1 < Ro < 100$ with $0 < Re < 500$, and it was found that the axial velocity is substantially distorted by the presence of secondary flow. More specifically, the axial velocity along the horizontal centreline of the duct was highly asymmetric, with its maximum value shifted toward the low-pressure side of the duct, and the axial velocity along the vertical centreline of the duct was flattened near the central portion of the duct. Furthermore, there was a substantial reduction in the flow rate as a result of the secondary flow. For all of the calculations presented herein where $Ro > 1$, the secondary flow consisted of the standard double-vortex configuration shown in figure (2*d*).

For slightly more rapid rotations (i.e. for $Ro < 1$) and sufficiently high Reynolds numbers ($Re \gg 1$) the double-vortex secondary flow was shown to break down into an asymmetric configuration of four counter-rotating vortices similar to that observed in curved rectangular ducts at higher Dean numbers. The axial velocity along the horizontal centreline of the duct was asymmetric as in the previous cases. However, in contrast, a point of inflexion appeared on the high-pressure side of the duct where roll-cell instabilities are observed in channel flow at comparable Rossby and Reynolds numbers. If the rotation rate is increased further, the flow restabilizes to a slightly asymmetric double-vortex configuration and the point of inflexion disappears in the axial velocity, which now assumes a Taylor–Proudman configuration in the interior of the channel. The numerical results obtained, which, to the best knowledge of the author, are the first calculations to demonstrate the breakdown of the double-vortex secondary flow and the restabilization to a Taylor–Proudman regime, appear to be in excellent agreement with experimental observations.

The analysis presented in this study tends to indicate that the presence of a subsidiary counter-rotating vortex pair on the high-pressure side of a 2×1 duct is a natural consequence of the Navier–Stokes equations (i.e. they result from a disparity in the symmetry of the convective and Coriolis terms). These subsidiary vortices occur when $Ro \sim 1$ and $Re \gg 1$. If a given axial flow is subjected to continuous increases in the angular velocity Ω, the flow will restabilize since the Reynolds number decreases as a result of the Coriolis terms, and consequently the convective terms become less dominant. It should be mentioned at this point that the four-vortex solution could constitute a bifurcation, i.e. a non-uniqueness of solutions. As discussed in §4, when the convective terms play a dominant role (i.e. when $Ro \sim 1$ and $Re \gg 1$) the classical *symmetric* double-vortex configuration for the secondary flow shown in figure 1 will cease to be a solution of the equations of motion. However, it is possible for an asymmetric double-vortex configuration (such as that shown in figure 11) to co-exist with the four-vortex configuration as non-unique solutions to the governing equations of motion. Such a bifurcation of solutions has been established for the case of laminar flow in a curved circular tube by Dennis & Ng (1982) in an interesting paper. More research would be needed to establish anything definitive concerning this issue of bifurcations in the present problem. Nevertheless, this is a topic that would be well worth pursuing in the future.

Future research is needed concerning the stability of this asymmetric four-vortex mode to longitudinal disturbances, since a point of inflexion occurs in the axial-velocity profiles. Such a study, which will be complicated because of the full three-dimensional form of the resulting disturbance equations, is beyond the scope of the present paper.

More experimental studies are also needed on rotating flow in low-aspect-ratio rectangular ducts for Rossby numbers $Ro \sim 1$. There is a noticeable lack of experimental data on this problem. In conclusion, the numerical results of this study indicate that there is a wealth of interesting physical phenomena associated with laminar flow in rotating rectangular ducts that are not fully understood. A better understanding of these phenomena is essential if real progress is to be made on the more complicated turbulent version of this problem which can have important technological applications in the design of turbomachinery.

The author would like to thank Dr Gareth Williams for some valuable comments concerning the numerical method used and Miss Joanne Fendell for running the computer programs. This work was supported by the National Science Foundation under Grant No. ENG 79-08180.

REFERENCES

Barua, S. N. 1954 Secondary flow in a rotating straight pipe. *Proc. R. Soc. Lond.* A **227**, 133–139.

Batchelor, G. K. 1967 *Introduction to Fluid Dynamics*. Cambridge University Press.

Benton, G. S. 1956 The effect of the earth's rotation on laminar flow in pipes. *J. Appl. Mech.* **23**, 123–127.

Benton, G. S. & Boyer, D. 1966 Flow through a rapidly rotating conduit of arbitrary cross-section. *J. Fluid Mech.* **26**, 69–79.

Buneman, O. 1969 A compact non-iterative Poisson solver. *Stanford Univ. Inst. for Plasma Res. Rep. SUIPR* no. 294.

Cheng, K. C., Lin, R. C. & Ou, J. W. 1976 Fully-developed laminar flow in curved rectangular channels. *Trans. A.S.M.E.* I, *J. Fluids Engng* **98**, 41–48.

Dennis, S. C. R. & Ng, M. 1982 Dual solutions for steady laminar flow through a curved tube. *Q. J. Mech. Appl. Math.* (to appear).

Hart, J. E. 1971 Instability and secondary motion in a rotating channel flow. *J. Fluid Mech.* **45**, 341–351.

Howard, J. H., Patankar, S. V. & Bordynuik, R. M. 1980 Flow prediction in rotating ducts using Coriolis-modified turbulence models. *Trans. A.S.M.E.* I, *J. Fluids Engng* **102**, 456–461.

Johnston, J. P., Halleen, R. M. & Lezius, D. K. 1972 Effects of spanwise rotation on the structure of two-dimensional fully developed turbulent channel flow. *J. Fluid Mech.* **56**, 533–557.

Lezius, D. K. & Johnston, J. P. 1976 Roll-cell instabilities in rotating laminar and turbulent channel flow. *J. Fluid Mech.* **77**, 153–175.

Majumdar, A. K., Pratap, V. S. & Spalding, D. B. 1977 Numerical computation of flow in rotating ducts. *Trans. A.S.M.E.* I, *J. Fluids Engng* **99**, 148–153.

Roache, P. J. 1972 *Computational Fluid Dynamics*. Hermosa.

Wagner, R. E. & Velkoff, H. R. 1972 Measurements of secondary flows in a rotating duct. *Trans. A.S.M.E.* A, *J. Engng Power* **95**, 261–270.